DOI: 10.31401/WS.2026.proc.19

Case Study of the First Forbush Decrease Detected by MNM ROZH Station

Tsvetkov Ts., Petrov N., Minev M.

Institute of Astronomy and National Astronomical Observatory, Bulgarian Academy of Sciences
tstsvetkov@nao-rozhen.org

Abstract

A mini neutron monitor station (MNM-ROZH) was recently deployed at the National Astronomical Observatory of the Bulgarian Academy of Sciences at 1730 m and has been operational since June 2025. The instrument includes three compact neutron monitor units equipped with BF_3 proportional counters (type LND2043). The main scientific goal of the instrument is to measure variations, including transients, of the incoming cosmic rays—high-energy particles produced in a variety of astrophysical environments, including explosive stellar phenomena and processes related to solar activity. They are composed mainly of protons, along with heavier nuclei and electrons, and their flux near Earth is strongly influenced by solar-driven disturbances in the heliosphere. We summarize the initial results from the first year of operation of the station. The reliability of the measurements is illustrated by the clear detection of a significant Forbush decrease in June 2025. These results demonstrate the station's capability to contribute to continuous cosmic ray monitoring and to studies of solar-terrestrial interactions.

Keywords: Mini Neutron Monitor; Ground-based Measurements; Cosmic Rays; Forbush Decrease

1. Introduction

Galactic cosmic rays (GCRs) constitute a persistent flux of high-energy charged particles reaching the heliosphere from sources outside the Solar System. Their propagation through interplanetary space is strongly influenced by the heliospheric magnetic field and by transient structures associated with solar activity. Consequently, the intensity of GCRs observed near Earth exhibits variations over a wide range of time scales, from the approximately 11-year solar cycle to short-term transient disturbances lasting from several hours to several days. Among the most prominent short-term variations are Forbush decreases (FDs), which provide an important means of investigating the interaction between solar disturbances and the GCR population.

A FD is generally defined as a transient reduction in the intensity of GCRs observed near Earth. The phenomenon was first reported by Forbush in the 1930s using ionization chambers [Forbush, 1937]. A typical FD is characterized by a relatively rapid decrease in cosmic ray (CR) intensity, followed by a more gradual recovery toward the pre-event level. The magnitude and temporal profile of an individual event can vary considerably, with some events showing a single-step decrease and others exhibiting a two-step structure. In the latter case, the first decrease is commonly associated with the turbulent sheath region preceding an interplanetary coronal mass ejection (ICME), while the second decrease can be related to the magnetic structure of the ejecta itself [Cane, 2000]. Although the detailed physical mechanisms responsible for individual FDs remain an active subject of research, the phenomenon is generally understood in terms of the modulation and transport of GCRs by disturbed heliospheric magnetic fields.

The connection between FDs and solar transients makes these events particularly useful for studying solar-terrestrial relations. Coronal mass ejections (CMEs) can substantially modify

the magnetic field configuration and particle transport conditions in the inner heliosphere. When an ICME and its associated shock propagate past the Earth, the enhanced magnetic turbulence and magnetic field strength can reduce the access of GCRs to the observer, producing a measurable decrease in the CR intensity [Cane, 2000]. The amplitude, duration, onset profile, and recovery phase of an FD therefore contain information about the interplanetary disturbance and about the rigidity-dependent propagation of CRs. In addition, comparisons of the same event at different observing locations can provide information about the spatial and rigidity dependence of the CR modulation [Lockwood, 1971].

Ground-based neutron monitors (NMs) have played a central role in the continuous observation of CR variability for more than half a century. Unlike direct measurements of primary CRs, NMs detect secondary particles generated when primary CR interact with nuclei in the Earth's atmosphere. High-energy primary particles initiate atmospheric nuclear cascades, producing secondary neutrons and other particles that can subsequently be detected at ground level. In a conventional NM, the neutrons are moderated and detected using gas-filled proportional counters, with the surrounding producer, moderator, and reflector providing the necessary neutron multiplication and detection efficiency [Simpson, 1957; Clem and Dorman, 2000].

The indirect nature of NM measurements is nevertheless one of their major strengths. Because the atmospheric cascade converts primary CR interactions into a large number of secondary particles, NMs provide high counting rates and consequently good statistical precision. Their continuous operation, relatively stable long-term response, and high temporal resolution make them particularly well suited to detecting small and rapid variations in CR intensity. The worldwide network of NMs also provides measurements at different geomagnetic latitudes, altitudes, and cutoff rigidities. This geographical distribution makes it possible to study the rigidity dependence of CR variations and to distinguish local or instrumental effects from large-scale changes in the GCR flux [Clem and Dorman, 2000; Okike et al., 2021].

Despite their scientific value, conventional NMs are relatively large, heavy, and resource-intensive instruments. A standard NM64-type monitor contains multiple proportional counters and a substantial amount of moderator, reflector, and neutron-producing material. These characteristics provide a high counting rate and stable response but make conventional NMs difficult to deploy at many locations. The resulting limitations in geographical coverage have motivated the development of more compact NM designs.

Mini-neutron monitors (MNMs) represent an important development in this direction. The MNM is essentially a portable implementation of the NM concept, designed to retain the essential detection principle while reducing the material requirements, physical dimensions, and operational complexity of a conventional instrument [Caballero-Lopez, 2016; Strauss et al., 2020]. An important advantage of MNMs is their potential for increasing the spatial density of CR monitoring stations. Strauss et al., (2020) emphasized that their relatively small size, reduced cost, and possibility of semi-autonomous operation make MNMs suitable for deployment in remote locations and for expanding the existing NM network. A denser network can improve the characterization of transient CR variations and contribute to near-real-time space weather monitoring. In particular, the detection of FDs by compact NMs demonstrates that such instruments can provide scientifically useful measurements of short-term GCR variability while complementing the observations obtained by established NM stations. This was our motivation to establish a MNM station at the National Astronomical Observatory Rozhen (Bulgaria). See more about the instrument in Section 2.

The detection of a FD by a ground-based NM therefore represents more than a simple decrease in the count rate. It provides a ground-based signature of a transient disturbance in the heliospheric environment and can be used, together with observations from other NMs

and space-based instruments, to investigate the propagation and impact of solar-driven interplanetary structures. The present work focuses on a case study of the first FD detected by the MNM ROZH station – the one from June 2025.

2. Mini-Neutron Monitor Station

The mini-neutron monitor station (MNM-ROZH) is installed at the National Astronomical Observatory Rozhen (41°41′ N, 24°44′ E, altitude: 1730 m) and provides continuous ground-based measurements of the secondary neutron component of CRs. The station consists of three independent MNM units based on BF_3 proportional counters (LND2043), operating according to the modern mini NM concept for long-term CR observations (see more about the technical parameters of the instrument in [Petrov et al., 2025; Tsvetkov et al., 2026]).

The detector is complemented by an integrated meteorological station that continuously records atmospheric pressure, temperature, relative humidity, precipitation, etc. These environmental measurements provide the basis for evaluating and, where appropriate, correcting local atmospheric effects on the neutron count rate.

Since becoming operational, MNM-ROZH has demonstrated stable long-term performance and the capability to register both gradual CR variations and transient events associated with space weather. The station is dedicated to the detection and analysis of Forbush effects and Ground Level Enhancement related studies and its real-time observations are integrated into the observatory data services and contribute to the international NM community.

3. Solar Origin and Interplanetary Conditions

The FD observed by MNM-ROZH between 31 May and 10 June 2025 occurred during a period of enhanced solar and interplanetary activity. In order to identify the solar drivers of the event, we considered the sequence of solar flares (SFs) and coronal mass ejections (CMEs) observed between 29 and 31 May, together with the subsequent solar wind (SW) and interplanetary magnetic field (IMF) conditions at Earth. CME times and kinematic parameters quoted below are taken primarily from SOHO/LASCO CME Catalog [Yashiro et al., 2004; Gopalswamy et al., 2024]. SF information is based on GOES/SIDC observations, while near-Earth SW and IMF parameters are taken from the ACE and DSCOVR observations and the NASA/GSFC OMNI data set [King and Papitashvili, 2005].

3.1. Preconditioning

The solar-terrestrial environment was already disturbed before the CME sequence associated with the June 2025 FD. On 29 May, a G3-level geomagnetic storm was observed in response to the arrival of a high-speed SW stream originating from an extended negative-polarity equatorial coronal hole [National Oceanic and Atmospheric Administration (NOAA) and National Weather Service (NWS) 2025a]. The coronal hole, identified as a combination of SIDC Coronal Holes 116 and 112, began crossing the solar central meridian on 26 May. The stream had begun to affect the near-Earth environment several days earlier and produced SW speeds of approximately 650–830 km s^{-1} on 30 May. The associated enhancement of the IMF reached about 24 nT, with B_z decreasing to approximately -24 nT during the initial high-speed-stream interaction [National Oceanic and Atmospheric Administration (NOAA) and National Weather Service (NWS) 2025b; Solar-Terrestrial Centre of Excellence (STCE) 2025]. This preceding high-speed stream is important for interpreting the subsequent CME-driven disturbance. It provided an already elevated SW background into which the CMEs of 30–31 May propagated. The 29 May disturbance should nevertheless be distinguished from the main FD studied here. In particular, the geomagnetic activity associated with the coronal hole high-speed stream preceded the abrupt CR decrease beginning on 1 June and did not exhibit the characteristic shock-associated CR depression observed during the later CME

passage. We therefore regard the coronal hole high-speed stream as a preconditioning agent rather than as the primary cause of the June 2025 FD.

3.2. Solar Activity of 30–31 May

Solar activity increased substantially on 30–31 May, primarily due to NOAA Active Region (AR) 4100. On 30 May, it produced three C-class SFs and an M3.4-class flare peaking at 06:13 UT. It was accompanied by an on-disk dimming and an Earth-directed CME first observed by SOHO/LASCO C2 at 07:12 UT [Solar Influences Data Analysis Center (SIDC) 2025a] with an angular width of 163° and a linear speed of 353 km s^{-1} and is classified as a partial halo CME [Gopalswamy et al., 2024]. Its wide angular extent and Earth-directed component make it a plausible precursor to the subsequent interplanetary disturbance, although its relatively low catalogued speed suggests that it could not by itself account for the unusually rapid shock observed at Earth on 1 June. Several other CMEs were also registered on 30 May. Their morphology, kinematics and propagation directions do not provide equally strong evidence for a direct Earth impact. Consequently, they are not considered primary candidates for the disturbance responsible for the observed FD.

The most significant solar eruption occurred shortly afterwards. AR 4100 produced a long-duration M8.1 flare peaking at 00:05 UT on 31 May. It occurred close to the solar central meridian and was accompanied by a Type II radio burst, coronal dimming, and a fast Earth-directed halo CME at 00:12:05 UT on 31 May [Solar Influences Data Analysis Center (SIDC) 2025b] (an angular width of 360° and a linear speed of 1752 km s^{-1} [Gopalswamy et al., 2024]). The combination of its full-halo morphology, high speed, source location close to the solar central meridian, and its direct association with the M8.1 flare makes this CME the strongest individual candidate for the major interplanetary disturbance observed at Earth on 1 June.

The temporal proximity of the 30 May and 31 May eruptions is also important. The much faster halo CME of 31 May was launched into a heliosphere already containing slower CME material from the preceding day. Independent space weather analyses therefore suggested that the fast CME could overtake the slower CME first observed on 30 May, resulting in an interacting or compound interplanetary structure [Solar Influences Data Analysis Center (SIDC) 2025b]. Such CME–CME interaction provides a plausible explanation for the unusually strong and extended SW disturbance observed at Earth.

3.3. First Interplanetary Disturbance

A clear interplanetary shock was detected near the Earth on 1 June at approximately 05:22 UT by both the ACE and DSCOVR spacecraft. The shock was characterized by an abrupt increase in the total IMF strength from approximately 7 nT to about 25 nT, accompanied by an increase in SW speed from approximately 700 km s^{-1} to more than 1100 km s^{-1}. The SW ion temperature also increased significantly, while the subsequent magnetic field evolution included a smooth rotation of the field components, consistent with the passage of structured ICME material [NASA Community Coordinated Modeling Center (CCMC) 2025b; King and Papitashvili, 2005].

The timing and magnitude of this disturbance provide strong evidence for its association with the CME sequence of 30–31 May. In particular, the CCMC/NASA analysis explicitly associates the 1 June 05:22 UT shock with the combined arrival of the CMEs observed on 30 May and the fast halo CME of 31 May [NASA Community Coordinated Modeling Center (CCMC) 2025b]. This interpretation is also consistent with independent space weather analyses, which associate the fast halo CME with the severe geomagnetic storm observed on 1 June. The geomagnetic response reached K_p=8 during the main phase of the storm, while

the minimum Dst value was approximately -120 nT [CDAW Data Center 2025; Solar-Terrestrial Centre of Excellence (STCE) 2025].

The arrival of this interplanetary structure is temporally consistent with the onset of the pronounced CR decrease observed by MNM-ROZH as well as other NMs. Thus, the first phase of the FD can be physically associated with the arrival of the shock and the following CME-driven sheath and magnetic structure. The enhanced magnetic field strength and turbulent conditions in these regions provide efficient scattering and exclusion of GCRs, producing the rapid decrease in NM count rates.

3.4. Subsequent Interplanetary Disturbance

The CR depression remained pronounced for several days after the first shock, indicating that the 1 June disturbance was followed by additional interplanetary structure rather than by an immediate return to undisturbed conditions. SW observations show a further interplanetary disturbance on 2 June at approximately 20:02 UT. At this time, the total magnetic field strength increased from an already elevated level of about 10 nT to 12.4 nT and subsequently to approximately 14.5 nT, while the SW speed increased from about 580 to 660 km s^{-1}. The event was detected by ACE and DSCOVR, although the corresponding ICME signature was classified as weaker than that of the 1 June event [NASA Community Coordinated Modeling Center (CCMC) 2025c].

The interplanetary medium remained disturbed after the arrival of the first CME complex. On 31 May, AR 4100 produced several additional M-class flares, including M2.4 and M4.5 and M2.9 SFs peaking at 05:18, 08:18 and 15:49 UT, respectively [Solar-Terrestrial Centre of Excellence (STCE) 2025]. No distinct fast Earth-directed CME associated with these two flares is identified in the SOHO/LASCO CME Catalog. A further CME was nevertheless catalogued by the NASA CCMC DONKI database with an event start time of 14:23 UT on 31 May. This event was observed by STEREO-A/COR2 and GOES/CCOR-1 and was reported only very faintly in SOHO/LASCO-C3; DONKI gives an estimated speed of approximately 680 km s^{-1} and an opening half-angle of about 35°. Its solar source is uncertain, although a small brightening and field-line motion near AR 4100 were identified as a possible source [NASA Community Coordinated Modeling Center (CCMC) 2025a]. A recent analysis of the same event using the SEVAN network identified a two-step FD and associated the two phases with sudden storm commencements at 05:22 UT on 1 June and 10:19 UT on 2 June [Karapetyan et al., 2026].

4. June 2025 Forbush Decrease

In this paper the CR response to the solar and interplanetary activity described in the previous section was investigated using the MNM-ROZH measurements and simultaneous observations from the Oulu and Rome NMs (Figure 1). To allow a direct comparison, the data from the three stations were averaged to a common temporal resolution of 60 min and expressed as relative variations with respect to their individual pre-event reference levels. The mean count rate on 30 May 2025 was adopted as the reference level, and the relative variation was calculated as

$$\Delta I(t) = \frac{I(t) - I_0}{I_0} \times 100\%, \quad (1)$$

where $I(t)$ is the hourly count rate and I_0 is the corresponding mean count rate during the reference interval.

4.1. Forbush decrease observed by MNM-ROZH

The MNM-ROZH measurements reveal a pronounced and prolonged decrease in the GCR intensity beginning on 1 June 2025 (Figure 1). Prior to the event, the count rate remained close to the reference level. During the morning of 1 June, however, a rapid decrease developed and the relative intensity fell below -10% during the afternoon. The onset of this decrease occurred within several hours of the strong interplanetary shock detected near Earth at approximately 05:22 UT, discussed in Section 3.

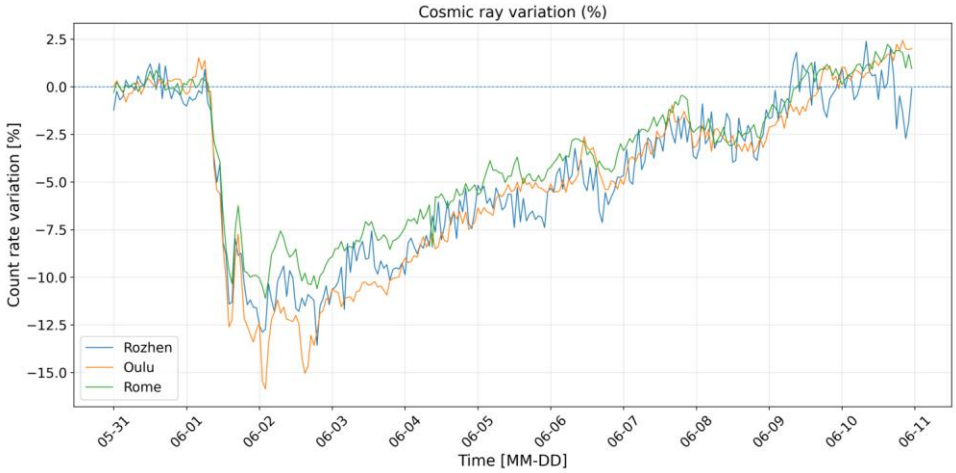


Figure 1. *Relative CR intensity variations recorded by the Rozhen, Oulu, and Rome NM stations from 31 May to 10 June 2025. The data are normalized to the mean count rate measured during the reference period on 30 May 2025, which is defined as 0% for each station. All data are corrected for the respective station response, and the measurements are presented at 1-hour temporal resolution.*

The subsequent evolution recorded at Rozhen shows a clear two-step structure – the first phase reached a minimum of approximately -12.85% at 01:00 UT on 2 June. During the following hours, the CR intensity partially recovered, reaching approximately -9.36% at 08:00 UT. This recovery was then interrupted by a renewed decrease during the second half of 2 June. The second depression reached a minimum of -13.53% at approximately 19:00 UT on 2 June. This represents the absolute minimum recorded by MNM-ROZH during the event. Relative to the preceding local recovery level, the second phase therefore corresponds to an additional CR suppression of approximately 4.17 percentage points. Interestingly, the second phase was slightly deeper than the first one in the MNM-ROZH measurements, with the two minima differing by approximately 0.68 percentage points. Following the second minimum, the CR intensity entered a prolonged recovery phase lasting several days – the overall trend was a gradual return toward the pre-event level, which was approached toward the end of the analysed interval.

4.2. Comparison with Oulu and Rome NMs

The identification of the event by MNM-ROZH is independently supported by the observations from the Oulu and Rome NMs. As shown in Figure 1, all three stations recorded a remarkably similar temporal evolution despite their different geographic locations, geomagnetic cut-off rigidities, and detector characteristics.

The first minimum is closely synchronized among the three stations (Table 1). MNM-ROZH reached a relative variation of -12.85% at approximately 01:00 UT on 2 June, while Oulu and Rome reached their first minima approximately one hour later, at 02:00 UT. The corresponding variations at Oulu and Rome were -15.87% and -11.11%, respectively. Given the common 60-min temporal resolution, the difference of one hour does not indicate a significant difference in the timing of the first minimum.

A particularly important feature is the partial recovery observed after the first minimum. The MNM-ROZH intensity increased to -9.36% by 08:00 UT. Similar local recoveries are independently observed at Oulu, where the intensity reached -11.19% at 06:00 UT, and at Rome, where it reached -7.56% at 07:00 UT. The simultaneous presence of this feature in all three records provides a natural separation between the two main phases of the event.

Following this partial recovery, the second decrease was not only detected by MNM-ROZH data. At Oulu, the second minimum of -15.05% occurred at approximately 15:00 UT. At both MNM-ROZH and Rome, the second minimum occurred at approximately 19:00 UT, reaching -13.53% and -10.60%, respectively. Relative to the local recovery preceding the second depression, the additional decreases were approximately 3.86, and 3.04 percentage points at Oulu, and Rome, respectively (4.17 for Rozhen; see 4.1).

The relative importance of the two phases is not identical at the three stations. At MNM-ROZH, the second minimum (-13.53%) was deeper than the first (-12.85%) and therefore represents the absolute minimum of the event. In contrast, the first minimum remained slightly deeper at Oulu (-15.87% compared with -15.05%) and Rome (-11.11% compared with -10.60%). Nevertheless, the overall morphology of the two-step decrease is highly consistent among the three stations.

The amplitude of the event also shows a systematic difference between the stations, with Oulu exhibiting the largest relative decrease, Rome the smallest, and MNM-ROZH an intermediate response. MNM-ROZH reproduces all of the major temporal features observed by the established Oulu and Rome stations. These include the rapid initial decrease, the first minimum, the intermediate recovery, the second depression, and the subsequent long-term recovery. The close agreement provides independent validation of the ability of MNM-ROZH to detect and characterize transient heliospheric modulations of GCRs.

Table 1. Characteristic parameters of the two-step Forbush decrease observed by MNM-ROZH, Oulu, and Rome. The partial-recovery value corresponds to the local maximum separating the two depressions. Times are given in UT.

Parameter	Rozhen	Oulu	Rome
First minimum time	2 Jun 01:00	2 Jun 02:00	2 Jun 02:00
First minimum	-12.85%	-15.87%	-11.11%
Partial-recovery time	2 Jun 08:00	2 Jun 06:00	2 Jun 07:00
Partial-recovery level	-9.36%	-11.19%	-7.56%
Second minimum time	2 Jun 19:00	2 Jun 15:00	2 Jun 19:00
Second minimum	-13.53%	-15.05%	-10.60%
Second-step decrease	4.17 p.p.	3.86 p.p.	3.04 p.p.

4.3. Relation to the interplanetary disturbances

The temporal evolution of the CR intensity can be compared with the sequence of interplanetary disturbances described in Section 3. The main decrease began shortly after the strong interplanetary shock detected near Earth at approximately 05:22 UT on 1 June. The rapid and nearly simultaneous response at MNM-ROZH, Oulu, and Rome strongly supports the association of the first phase of the FD with the arrival of the CME-driven disturbance and the subsequent passage of the disturbed interplanetary structure.

Following the first minimum, all three stations show a significant but temporary recovery during the early hours of 2 June. This recovery is followed by a coherent renewed decrease, producing a second minimum later the same day. The presence of the same sequence at three geographically separated NM stations demonstrates that the second depression represents a large-scale modulation of the GCR flux rather than a local or instrumental variation. The

temporal correspondence supports the interpretation of the event as a two-step, or more generally multi-phase, FD. As previously discussed in Section 3, the NM observations provide strong evidence for a two-step CR response, while the identification of a unique solar driver for the second step remains uncertain. A similar two-step structure of the 1–2 June 2025 FD has also been reported independently from observations of the SEVAN particle detector network [Karapetyan et al., 2026].

5. Conclusions

The available observations support a scenario in which the June 2025 FD was produced by a sequence of interacting solar eruptions rather than by a single isolated CME. The 29 May coronal hole high-speed stream established an already disturbed solar wind background. The M3.4-associated CME observed by LASCO on 30 May provided a slower, wide Earth-directed structure, followed by the much faster full-halo CME associated with the M8.1 flare on 31 May. The latter likely interacted with and overtook preceding CME material during interplanetary propagation, resulting in a complex CME-driven structure whose arrival at Earth was observed as a strong interplanetary shock on 1 June.

The temporal correspondence between this shock, the abrupt increase in the IMF strength and SW speed, and the onset of the CR depression provides a strong physical basis for identifying the 1 June interplanetary disturbance as the principal driver of the observed FD. The subsequent interplanetary disturbance on 2 June coincided with a renewed suppression of the CR intensity following a short partial recovery. However, its association with a specific solar eruption is considerably less certain, since no unambiguous corresponding Earth-directed CME can be identified in the SOHO/LASCO CME Catalog. The second phase may therefore reflect an additional perturbation propagating through the already disturbed interplanetary medium and/or the internal evolution and interaction of structures within the complex ICME environment.

The MNM-ROZH observations reveal a pronounced two-step structure of the FD. The first minimum of -12.85% was reached at approximately 01:00 UT on 2 June, followed by a partial recovery to -9.36% at 08:00 UT. The CR intensity subsequently decreased again by approximately 4.17 percentage points, reaching the absolute event minimum of -13.53% at approximately 19:00 UT. The event was followed by a prolonged and non-monotonic recovery extending over several days.

Comparison with the Oulu and Rome NMs confirms that the principal temporal features observed at Rozhen were not local or instrumental in origin. All three stations recorded the rapid initial decrease, a closely synchronized first minimum, the intermediate partial recovery, and a second depression on 2 June. The observed amplitude differences are qualitatively consistent with the different geomagnetic cut-off rigidities and detector response functions of the three stations. Despite these differences, the close agreement in the temporal evolution demonstrates that MNM-ROZH reliably traces the large-scale modulation of GCRs during the event.

The June 2025 event represents the first FD detected by MNM-ROZH. Although it is a recently established MNM with lower counting statistics than conventional stations, its response to the disturbance is consistent with independent observations from other stations. In particular, the instrument successfully resolved not only the main CR depression but also the more complex two-step structure and subsequent recovery. These results demonstrate the capability of MNM-ROZH to provide reliable observations of transient CR variations and support its use for future studies of FDs and other space weather related phenomena.

Acknowledgements

The research that led to these results was partially carried out with the help of infrastructure purchased under the National Roadmap for Research Infrastructure, financially coordinated by the Ministry of Education and Science of Republic of Bulgaria.

We acknowledge the NMDB database (www.nmdb.eu) founded under the European Union's FP7 programme (contract no. 213 007), and the PIs of individual neutron monitors at: Rome (SVIRCO Observatory, INAF IFSI-UNIRomaTre, Italy), Oulu (Sodankyla Geophysical Observatory of the University of Oulu, Finland).

The SOHO/LASCO CME catalog is generated and maintained at the CDAW Data Center by NASA and The Catholic University of America in cooperation with the Naval Research Laboratory. SOHO is a project of international cooperation between ESA and NASA.

References

Caballero-Lopez, R.A. (2016). An estimation of the yield and response functions for the mini neutron monitor, *Journal of Geophysical Research: Space Physics*, Vol. 121, No. 8, pp. 7461–7469, DOI: 10.1002/2016JA022690.

Cane, H.V. (2000). Coronal mass ejections and Forbush decreases, *Space Science Reviews*, Vol. 93, Nos. 1–2, pp. 55–77, DOI: 10.1023/A:1026532125747.

CDAW Data Center (2025). List of intense geomagnetic storm events, NASA Goddard Space Flight Center, Coordinated Data Analysis Workshops Data Center. Available at: https://cdaw.gsfc.nasa.gov/CME_list/dst100/.

Clem, J.M., Dorman, L.I. (2000). Neutron monitor response functions, *Space Science Reviews*, Vol. 93, Nos. 1–2, pp. 335–359, DOI: 10.1023/A:1026508915269.

Forbush, S.E. (1937). On the effects in cosmic-ray intensity observed during the recent magnetic storm, *Physical Review*, Vol. 51, No. 12, pp. 1108–1109, DOI: 10.1103/PhysRev.51.1108.3.

Gopalswamy, N., Michałek, G., Yashiro, S., Mäkelä, P., Akiyama, S., Xie, H., Vourlidas, A. (2026). The SOHO LASCO CME Catalog – Version 2, *Proceedings of the International Astronomical Union*, Vol. 20, Symposium S388, pp. 133–139, DOI: 10.1017/S1743921325000559.

Karapetyan, T., Chilingarian, A., Sargsyan, B. (2026). SEVAN network observations of the complex Forbush decrease on 1–2 June 2025, *New Astronomy*, Art. 102622, DOI: 10.1016/j.newast.2026.102622.

King, J.H., Papitashvili, N.E. (2005). Solar wind spatial scales in and comparisons of hourly Wind and ACE plasma and magnetic field data, *Journal of Geophysical Research: Space Physics*, Vol. 110, No. A2, Art. A02104, DOI: 10.1029/2004JA010649.

Lockwood, J.A. (1971). Forbush decreases in the cosmic radiation, *Space Science Reviews*, Vol. 12, No. 5, pp. 658–715, DOI: 10.1007/BF00173346.

NASA Community Coordinated Modeling Center (CCMC) (2025a). DONKI: Coronal mass ejection, 31 May 2025, 14:23 UT, *Space Weather Database of Notifications, Knowledge, Information*. Available at: https://kauai.ccmc.gsfc.nasa.gov/DONKI/view/CME/39225/1.

NASA Community Coordinated Modeling Center (CCMC) (2025b). DONKI: Interplanetary shock/CME arrival, 1 June 2025, 05:22 UT, *Space Weather Database of Notifications, Knowledge, Information*. Available at: https://kauai.ccmc.gsfc.nasa.gov/DONKI/view/IPS/39238/2.

NASA Community Coordinated Modeling Center (CCMC) (2025c). DONKI: Interplanetary shock/CME arrival, 2 June 2025, 20:02 UT, *Space Weather Database of Notifications, Knowledge, Information*. Available at: https://kauai.ccmc.gsfc.nasa.gov/DONKI/view/IPS/39265/4.

National Oceanic and Atmospheric Administration (NOAA), National Weather Service (NWS) (2025). G3 level geomagnetic event observed, *NOAA Space Weather Prediction Center*. Available at: https://www.spaceweather.gov/news/g3-level-geomagnetic-event-observed-0.

Okike, O., Alhassan, J.A., Iyida, E.U., Chukwude, A.E. (2021). A comparison of catalogues of Forbush decreases identified from individual and a network of neutron monitors: A critical perspective, *Monthly Notices of the Royal Astronomical Society*, Vol. 503, No. 4, pp. 5675–5691, DOI: 10.1093/mnras/stab680.

Petrov, N., Tsvetkov, T., Mishev, A., Yotov, V., Shirov, G. (2025). First observational data from the mini-neutron monitoring station at the Rozhen National Astronomical Observatory (MNMS-ROZH), *Publications of the Astronomical Observatory of Belgrade*, Vol. 107, pp. 37–42, DOI: 10.69646/14sbac05p.

Simpson, J.A. (1957). Cosmic-radiation neutron intensity monitor, *Annals of the International Geophysical Year*, Vol. 4, pp. 351–373, DOI: 10.1016/B978-1-4832-1304-0.50020-8.

Solar Influences Data Analysis Center (SIDC) (2025a). Bulletin on solar and geomagnetic activity – 30 May 2025, Royal Observatory of Belgium/SIDC. Available at:

https://www.spaceweatherlive.com/en/archive/2025/05/30/sidc-ursigram.html.

Solar Influences Data Analysis Center (SIDC) (2025b). Bulletin on solar and geomagnetic activity – 31 May 2025, Royal Observatory of Belgium/SIDC. Available at: https://www.spaceweatherlive.com/en/archive/2025/05/31/sidc-ursigram.html.

Solar-Terrestrial Centre of Excellence (STCE) (2025). Fast CME, severe geomagnetic storm, *STCE Newsletter*. Available at: https://www.stce.be/newsletter/html/2025/STCEnews20250605.html.

Strauss, D.T., Poluianov, S., van der Merwe, C., Krüger, H., Diedericks, C., Krüger, H., Usoskin, I., Heber, B., Nndanganeni, R., Blanco-Ávalos, J.J., García-Tejedor, I., Herbst, K., Caballero-Lopez, R.A., Moloto, K., Lara, A., Walter, M., Giday, N.M., Traversi, R. (2020). The mini-neutron monitor: A new approach in neutron monitor design, *Journal of Space Weather and Space Climate*, Vol. 10, Art. 39, DOI: 10.1051/swsc/2020038.

Tsvetkov, Ts., Petrov, N., Mishev, A., Poluianov, S., Minev, M. (2026). New mini neutron monitor at National Astronomical Observatory Rozhen: First measurements, *Advances in Space Research*, Vol. 78, No. 6, pp. 6634–6643, DOI: 10.1016/j.asr.2026.07.017.

Yashiro, S., Gopalswamy, N., Michalek, G., St. Cyr, O.C., Plunkett, S.P., Rich, N.B., Howard, R.A. (2004). A catalog of white light coronal mass ejections observed by the SOHO spacecraft, *Journal of Geophysical Research: Space Physics*, Vol. 109, No. A7, Art. A07105, DOI: 10.1029/2003JA010282.